J Mol Model (2013) 19:5053–5062
DOI 10.1007/s00894-013-1996-4

ORIGINAL PAPER

Molecular dynamics simulation of cross-linked urea-formaldehyde polymers for self-healing nanocomposites: prediction of mechanical properties and glass transition temperature

Behrouz Arab · Ali Shokuhfar

Received: 24 July 2013 / Accepted: 4 September 2013 / Published online: 1 October 2013

Abstract Urea-formaldehyde polymers, which are utilized in the adhesives industry, have recently been shown to be suitable materials for synthesizing micro/nanocapsules for use in self-healing (nano)composites. In this study, molecular dynamics was employed to simulate the process in which urea and formaldehyde are cross-linked via methylene and ether cross linkers, and to study the structure and mechanical/thermal properties of simulated poly(urea-formaldehyde)s (PUFs). The elastic stiffness constants of the simulated materials were calculated using the constant-strain (static) method. A temperature cycle was applied to the cross-linked PUFs, and the glass transition behavior of each material was investigated through the mean squared displacement (MSD) and temperature evolution of the energy and the specific volume of the polymer. The simulation results confirmed that there was considerable improvement in the properties of the poly(UF) materials upon cross linking. The radial distribution function was also used to study the local structures of the polymers, and this revealed that increasing the temperature and cross linking density results in a significant drop in hydrogen bonding intensity in the cross-linked PUF systems.

Keywords Cross linking · Elastic constants · Glass transition temperature · Molecular dynamics · Self-healing materials · Urea-formaldehyde

B. Arab (✉) · A. Shokuhfar
Advanced Materials and Nanotechnology Research Lab, Faculty of Mechanical Engineering, K. N. Toosi University of Technology, P.O. Box: 19395–1999, Tehran, Iran
e-mail: arab@dena.kntu.ac.ir

Introduction

The idea of microcapsule-based self-healing materials was introduced in 2001 by White et al. [1]. Since then, this concept has been widely used in various research studies [2–7]. In brief, micro/nanocapsules containing the healing agent (e.g., dicyclopentadiene) together with a proper catalyst (either in powder form or stored in capsules) are dispersed in a polymer matrix. Initiating and propagating cracks in the matrix causes the capsule shell to rupture, releasing the healing agent. Curing the released agent in the presence of a catalyst prevents the crack from propagating any further, and subsequently restores the functionality and mechanical properties of the material.

Urea-formaldehyde polymers have reasonably high strength and stability, meaning that they can be used to store and isolate the healing agent from its surrounding matrix material. Hence, they are the most frequently used polymers in the synthesis of capsules for self-healing materials. The production of urea–formaldehyde polymers is typically carried out in two stages:

(i) *Addition polymerization*, also known as *methylolation* or *hydroxymethylation*, under neutral or alkaline conditions; in this case, a series of reactions between formaldehyde molecules and amino groups of urea molecules leads to the formation of mono-, di-, and trimethylol urea pre-polymers. Tetramethylol urea does not appear, at least not in detectable quantities [8].

(ii) *Condensation polymerization* or *polycondensation* under acidic conditions, leading to the formation of polymer chains and cross-linked networks via methylene ($-CH_2-$) and dimethylene ether ($-CH_2-O-CH_2-$) linkages

between previously created methylol (hydroxymethyl) urea pre-polymers.

This procedure can be effectively utilized in the synthesis of urea-formaldehyde capsules for self-healing materials. The duration of the process, the amine to formaldehyde ratio, and the alkalinity of the medium determine the chemical composition and structure of the pre-polymers, and have crucial influences on the stability of the microcapsules [8]. Excessive basicity and long reaction times must be eliminated during the first stage to prevent unwanted polymerization of methylol urea pre-polymers before the core–shell formation stage. The formation of dimethylene ether linkages is not desirable, as they would lower the functionality of the system and consequently the cross linking density of the product, which is detrimental to capsule wall strength [9]. Therefore, the second stage should be carried out under acidic conditions and in the presence of the core material (healing agent), so that the stronger and more favorable methylene linkages are dominantly created between the methylol urea pre-polymers, and a highly cross-linked UF shell is obtained around the core material.

In the study described in the present paper, molecular dynamics (MD) was used for the first time to simulate the cross linking of urea-formaldehyde polymers via methylene and ether cross linkers, as well as to study the mechanical properties and glass transition behavior of the simulated polymers. The effects of the cross linkers (methylene or ether) and the temperature on the structure and properties of the urea-formaldehyde polymers were also investigated. The principal aims of this study were to obtain deep insight into the structure and properties of PUF materials and to extract useful information for synthesizing poly(urea-formaldehyde) micro/nanocapsules for self-healing materials.

Methylol urea pre-polymers and cross-linked poly(UF)

The primary molecular structures of urea and formaldehyde are represented schematically in Fig. 1 (top). The C=O double bond in the formaldehyde molecule needs to be converted to a single bond in order to form a reactive $-CH_2$ site that is capable of reacting with amine groups of the urea molecule (Fig. 1). In the primary blend of urea and formaldehyde, under appropriate pH and temperature conditions, the curing sites can get sufficiently close to each other to facilitate the creation of covalent bonds between C and N atoms, leading to the formation of mono-, di-, and trimethylol urea pre-polymers (methylolation or hydroxymethylation). In the next stage, under acidic conditions, cross-linked urea-formaldehyde polymers are obtained. Figure 2 illustrates the formation of methylol urea pre-polymers from urea and formaldehyde molecules and subsequently the generation of UF chains from pre-polymers through addition and condensation polymerizations, respectively. Dimethylene ether

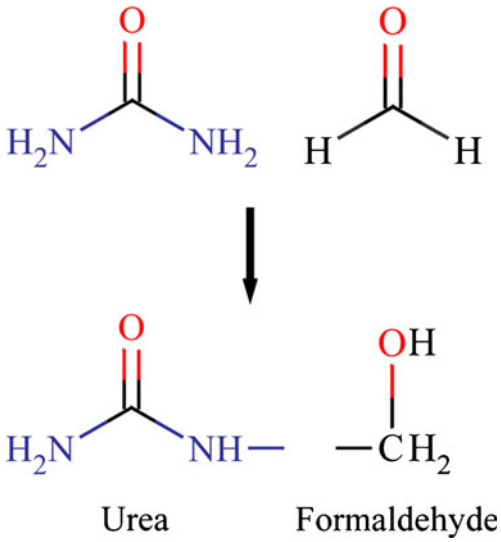

Fig. 1 Schematic representation of urea and formaldehyde molecules in their original (*top*) and activated (*bottom*) states

linkages are mainly created between two methylol groups. Methylene linkages, however, can be created in three ways: directly between methylol and amino groups, directly between two methylol groups that split off formaldehyde molecules, and by liberating formaldehyde molecules from previously created ether linkages. The condensation reactions that most likely result in the formation of UF polymers via methylene and ether linkages are discussed in [10].

As can be seen in Fig. 2, there are one primary amine ($-NH_2$) and one secondary amine (−NH−) in monomethylol urea, two secondary amines in *N*,*N*′-dimethylol urea, and one secondary amine and one tertiary amine (*N*) in trimethylol urea. The ratio of the rates for the addition of formaldehyde to form one, two, and then three methylol groups is estimated to be 9:3:1 [11] due to the different activation energies of the primary, secondary, and tertiary amines. Based on this ratio, the approximate ratio of relative abundances of the mono-, di-, and trimethylol ureas is thought to be 9:3:1.

Modeling and simulation

Software and force field

The Materials Studio 5.5 software package from Accelrys Inc. [12] was used to perform the modeling and molecular mechanics (MM)/dynamics (MD), along with the freely available LAMMPS (Large-scale Atomic/Molecular Massively Parallel Simulator) [13] MD package from Sandia National Labs [14].

The polymer consistent force field (PCFF) [15] was used at all stages of the modeling and simulation. The class II force field, PCFF was developed from CFF91 and parameterized for various polymers and organic materials. It can also be used

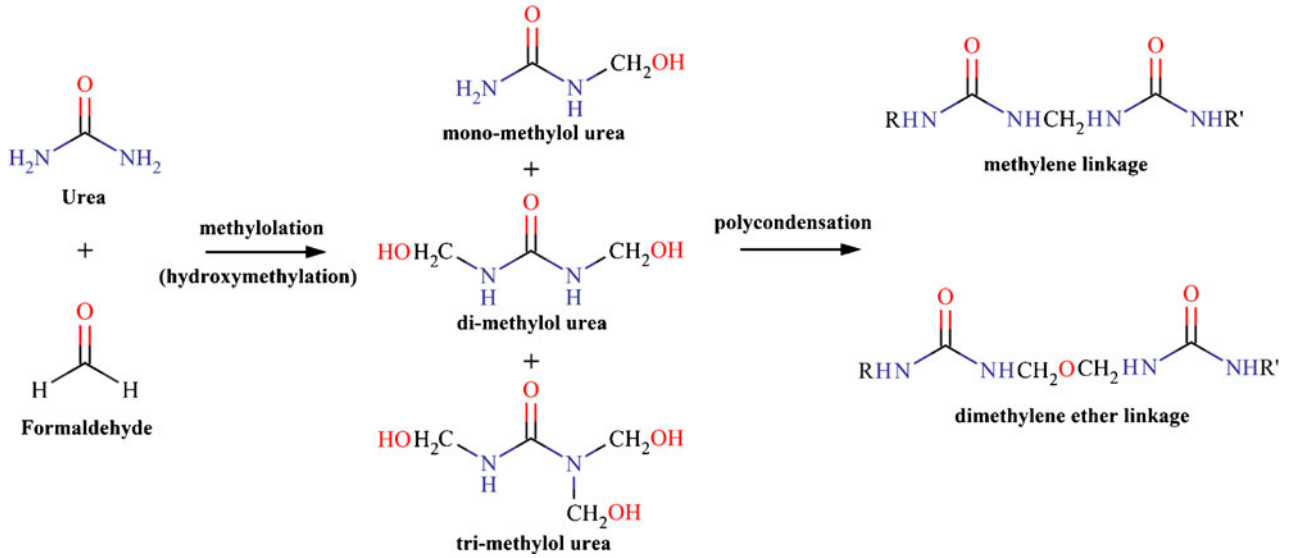

Fig. 2 The addition and condensation polymerization reactions that lead to the formation of methylol urea pre-polymers from urea and formaldehyde molecules and the generation of UF chains from pre-polymers, respectively

to calculate cohesive energies, mechanical properties, compressibilities, heat capacities, and elastic constants.

The nonbonded interactions, including the relatively short-range van der Waals (vdW) and long-range electrostatic interactions, were described using the Lennard–Jones (LJ) 9–6 and Coulombic functions, respectively. The atom-based summation method with a cut-off radius of 10 Å and long-range corrections was used when calculating the vdW interactions, while electrostatic interactions were handled using the Ewald summation method [16] with an accuracy of 0.0001 kcal/mol^{-1}.

Cross linking procedure

The cross linking procedure that was applied to simulate urea-formaldehyde polymers is based on the method provided in our previous study [17]:

Step 1. *Formation of pre-polymers*.

A series of molecular mechanics and dynamics simulations were performed to create short representative chains of pre-polymers. An amorphous cell composed of 25 urea and 25 formaldehyde molecules with a density of 0.5 g/cm^3 was constructed at room temperature. Energy minimization was carried out using a conjugate gradient algorithm, followed by 300 ps NPT dynamics at room temperature and atmosphere pressure for equilibration. Based on a predefined cut-off distance of 6 Å, close contacts between reactive sites of the urea (N) and formaldehyde (C) molecules were identified, and covalent bonds were created. The resulting structure was again minimized to release the stress imposed during the bond creation stage. Analyzing the resulted structure, mono-, di-, and trimethylol urea pre-polymers were identified and extracted as single, independent molecules for use in subsequent steps to create cross-linked urea-formaldehyde networks.

Step 2. *Pre-equilibration*.

An amorphous cell containing 90 mono-, 30 di-, and 10 trimethylol ureas (based on the ratio of formation rates of pre-polymers, 9:3:1) was constructed at room temperature and under periodic boundary conditions with a low density of 0.5 g/cm^3. The system was subjected to energy minimization through both steepest descent and conjugate gradient (Fletcher–Reeves) algorithms, with convergence criteria of 1000 and 10 kcal/mol Å, respectively. Afterward, the minimized amorphous cell was submitted to 500 ps dynamics in the isothermal-isobaric (NPT) ensemble at room temperature and atmosphere pressure to achieve the real density and equilibration. A time step of 1 fs was considered. The Berendsen thermostat and barostat [18] were used to control, respectively, the temperature and pressure of the system. Equilibration was considered to have occurred when the potential energy, temperature, and density of the system remained stable with only slight fluctuations around the target values.

Two extra copies of the equilibrated structure were generated. In the rest of this paper, these models will be referred to as UF0, UF1, and UF2. UF0 was not cross-linked, while UF1 and UF2 were cross-linked using different cross linking strategies.

Step 3. *Creation of covalent bonds*.

This step was in fact equivalent to the condensation polymerization stage in which cross-linked urea-formaldehyde networks are created. Cross linking of

UF1 was carried out solely via the methylene linkages, which is preferable for self-healing materials. UF2, however, was cross-linked via both methylene and dimethylene ether linkages. Both cases were adjusted to reach nearly the same degrees of cross linking.

A value of 6 Å [17] was adopted as the cross linking cut-off distance. Starting from the equilibrated structures, the distances between pairs of reactive atoms were measured, and covalent bonds were created between the atoms within the cross linking cut-off distance. Energy minimization was then performed in order to release the stress imposed on the systems. After minimization, the systems were subjected to 100 ps high-temperature NVT dynamics at 500 K, in order to supply enough kinetic energy to the molecules and increase the probability of curing sites falling within the reaction cut-off distance. Again, the distances between pairs of remaining reactive atoms were measured, and new covalent bonds were created, if possible. As the cross linking proceeded, the number of reactive sites and thus the possibility of new bonds being created decreased and finally approached zero. The final structures were analyzed, and 129 methylene cross links were identified in total in UF1, while UF2 contained 90 methylene and 39 ether cross links. It should be noted here that the main limit on the cross linking process is the assigned cross linking cut-off distance. In other words, the maximum number of cross links attainable is restricted by the cut-off value, since the creation of covalent bonds can occur solely within a predefined cut-off distance around the reaction sites. Although longer reaction cut-off distances could be used to increase the maximum attainable degrees of cross linking, the structures obtained will be highly stressed and difficult to equilibrate.

Step 4. *Post-equilibration and sampling*.

The final cross-linked UF1 and UF2 structures were gradually cooled to room temperature at a rate of 20 K/100 ps in the NVT ensemble, and were then equilibrated through 500 ps NPT dynamics using the same procedure as in step 2.

Finally, all three equilibrated systems were subjected to 300 ps NVT dynamics with a time step of 1 fs, and the configurations generated were stored every 1 ps as the sampling trajectories for further analysis and calculation of the properties. The Nosé–Hoover thermostat [19, 20] was employed to control the temperature during the sampling stage. The final structures of the uncross-linked UF0 and the cross-linked UF1 and UF2 models are represented in Fig. 3.

Calculation of the properties

Mechanical properties

Assuming a fixed bond length and angle during deformation, and negligible effects of configurational entropy on the elastic constants, the constant-strain (static) method [21] was used in this study to calculate the mechanical properties of the simulated polymers. Calculation of the mechanical properties was initiated by pre-minimizing the structures to make sure that the calculations were based on the most stable configurations. The minimized structures was strained under a set of 12 deformations (three pairs of uniaxial tension/compression and three pairs of pure shear), which were controlled by the corresponding strain vectors. One component took a tiny value while the others were fixed at zero and then re-minimized without changing the cell parameters. The maximum strain amplitude was set to ±0.003. Then the stress components were calculated using the so-called virial expression:

$$\sigma_{ij} = -\frac{1}{V}\sum_{k}\left(m^{k}\left(u_{i}^{k}u_{j}^{k}\right)+\frac{1}{2}\sum_{l\neq k}\left(r_{i}^{kl}\right)f_{j}^{lk}\right), \quad (1)$$

with the first term on the right hand side omitted because of the static conditions. Here, V is the volume, m^k and u^k denote the mass and velocity of the k^{th} particle, respectively, r^{kl}

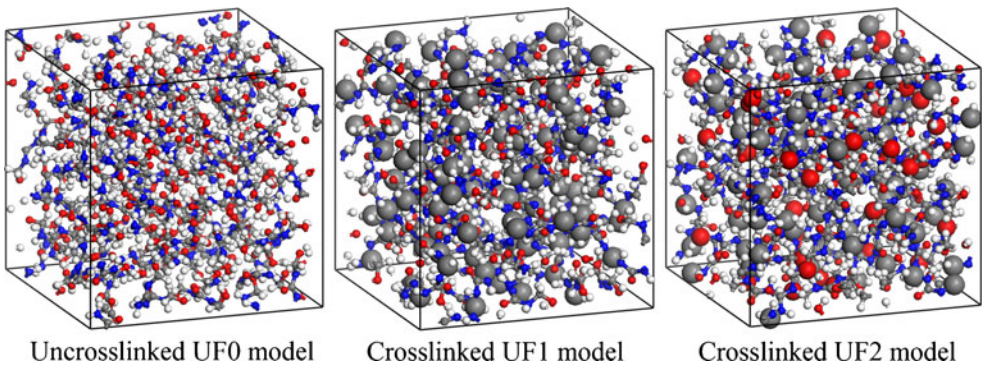

Fig. 3 Snapshots of the uncross-linked UF0 model (*left*), the cross-linked UF1 model with methylene linkages (*middle*), and the cross-linked UF2 model with both methylene and ether linkages (*right*). The *gray-colored* C atoms and *red-colored* O atoms in CPK style correspond to methylene and ether linkages, respectively

Table 1 Comparison of the densities and elastic properties of simulated urea-formaldehyde polymers with the corresponding values obtained experimentally (all moduli values are in GPa)

Property	Simulation results			Experimental results	
	UF0	UF1	UF2	From [23]	From [24]
Density (g/cm^3)	1.40	1.49	1.46	1.50	–
Elastic modulus, E	7.42	11.93	11.11	7–10.50	8.35–10.25[a] 6.55–8.45[b]
Bulk modulus, K	6.37	9.86	9.12	–	–
Shear modulus, G	2.84	4.60	4.28	–	–
Poisson's ratio, ν	0.31	0.30	0.30	–	–

[a] Reduced elastic modulus, E_r

[b] Calculated elastic modulus, E_s

stands for the distance between the k^{th} and l^{th} particles, and f^{lk} is the force exerted on the l^{th} particle by the k^{th} particle. The elastic stiffness constants were then obtained using the first derivative of the virial stress with respect to the strain, $\partial\sigma/\partial\varepsilon$. In other words, the full 6×6 stiffness matrix was built up from the slopes of $\partial\sigma/\partial\varepsilon$ under tension and shear. Afterward, the Lamé coefficients λ and μ were calculated from the stiffness matrix using the following equations:

$$\mu = \frac{1}{3}(C_{44} + C_{55} + C_{66}) \tag{2a}$$

$$\lambda + 2\mu = \frac{1}{3}(C_{11} + C_{22} + C_{33}). \tag{2b}$$

On the other hand, the stress–strain behavior of isotropic materials can be fully described using two independent Lamé coefficients:

$$\begin{pmatrix} \lambda+2\mu & \lambda & \lambda & 0 & 0 & 0 \\ \lambda & \lambda+2\mu & \lambda & 0 & 0 & 0 \\ \lambda & \lambda & \lambda+2\mu & 0 & 0 & 0 \\ 0 & 0 & 0 & \mu & 0 & 0 \\ 0 & 0 & 0 & 0 & \mu & 0 \\ 0 & 0 & 0 & 0 & 0 & \mu \end{pmatrix}. \tag{3}$$

A patterned combination of the zero and nonzero components in Eq. 3 and symmetry of the matrix along the diagonal components are the main characteristics of an isotropic material. The other material properties were calculated from the Lamé coefficients using the following equations:

$$E = \frac{\mu(3\lambda + 2\mu)}{\lambda + \mu} \tag{4a}$$

$$K = \lambda + \frac{2}{3}\mu \tag{4b}$$

$$G = \mu \tag{4c}$$

$$\nu = \frac{\lambda}{2(\lambda + \mu)}, \tag{4d}$$

where E, K, and G are Young's, bulk and shear moduli, respectively, and ν denotes Poisson's ratio.

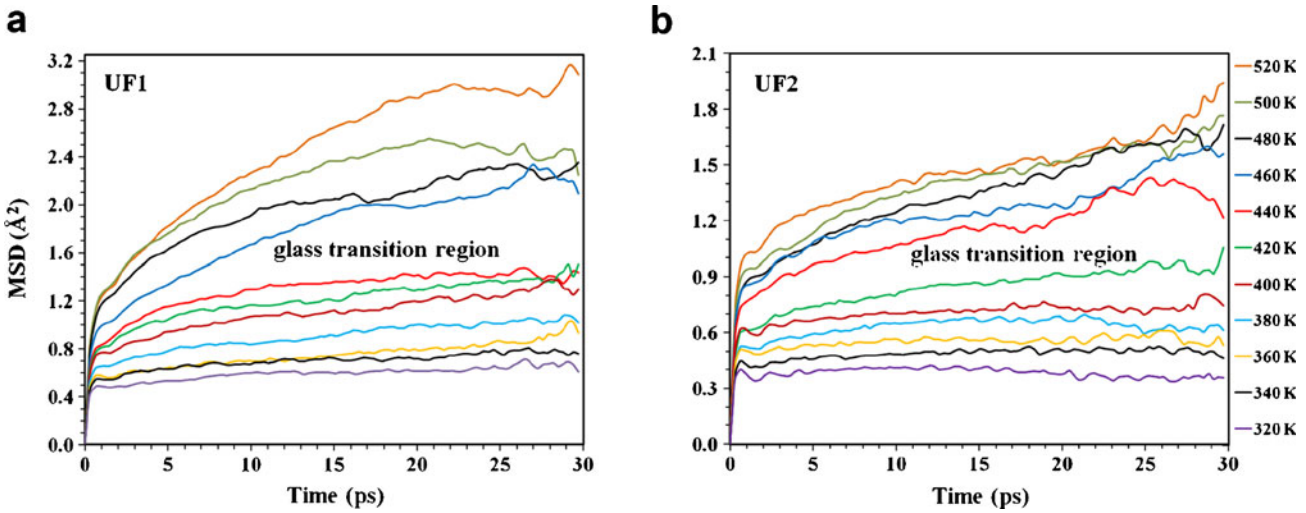

Fig. 4a–b MSD–time curves of cross-linked **a** UF1 and **b** UF2 at different temperatures ranging from 320 to 520 K. The large gap between the "lower set" and "upper set" of MSD curves in each plot indicate the glass transition region of the polymer (as marked on each plot)

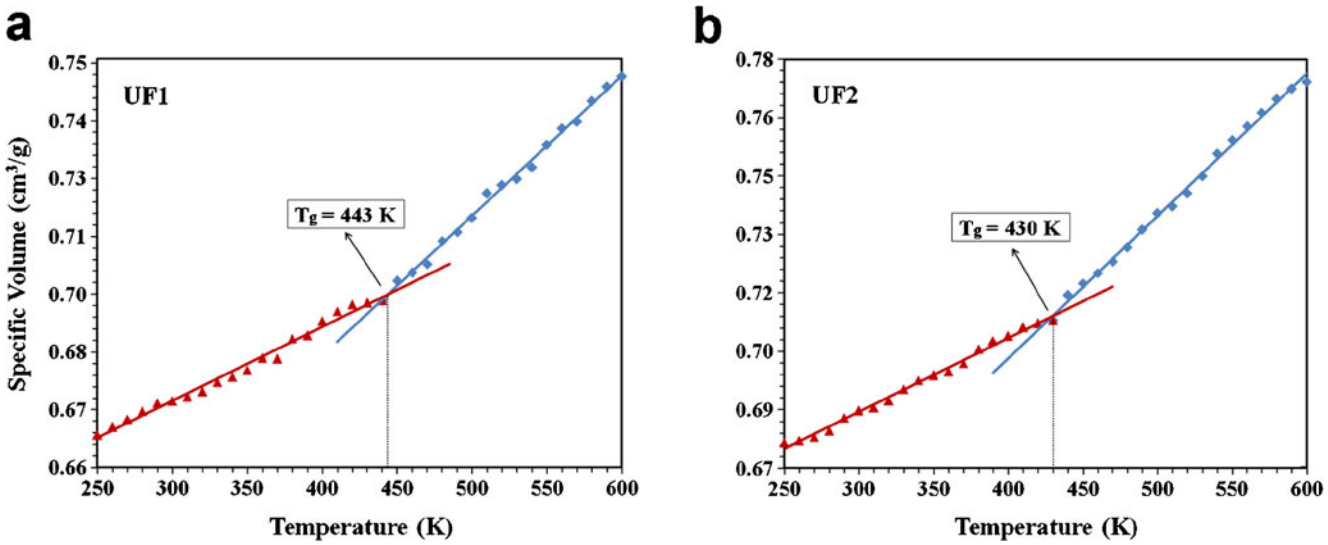

Fig. 5a–b Variation of the specific volume with respect to temperature for **a** UF1 and **b** UF2. The point of intersection between the fitted lines provides an estimate of the glass transition temperature (as shown on each plot)

Glass transition behavior

The glass transition temperature (T_g) is the point at which the behavior of a polymer changes from that of a glassy and relatively brittle state to a rubbery state. In the field of polymer science and technology, T_g is of crucial importance, as it determines the temperature ranges in which polymers can be processed and applied. Differential scanning calorimetry (DSC), differential thermal analysis (DTA), thermomechanical analysis (TMA), dynamic mechanical analysis (DMA), and dilatometry (DIL) are the main experimental methods for determining the glass transition temperature. There are three typical approaches that can be used to find T_g through the MD simulations: (i) the *mean squared displacement* (*MSD*), (ii) the *energy–temperature approach*, and (iii) the *property–temperature approach*.

The MSD for a system of N atoms can be described by the following expression:

$$\mathrm{MSD} = \frac{1}{3N}\sum_{i=0}^{N-1}\left\langle \left| \vec{\mathbf{r}}_i(t) - \mathbf{r}_i(t_0) \right|^2 \right\rangle, \quad (5)$$

where $\mathbf{r}_i(t)$ represents the position vector of the i^{th} atom at time t. The diffusivity of molecular system can be estimated through the MSD. When a polymer undergoes a glassy to rubbery phase transition, the torsional and rotational motions of the molecules combined with the local motion can cause chain disentanglement, leading to a sudden increase in the diffusivity and consequently a sudden jump in the MSD–time curves obtained at a range of temperatures [22]. Therefore, the

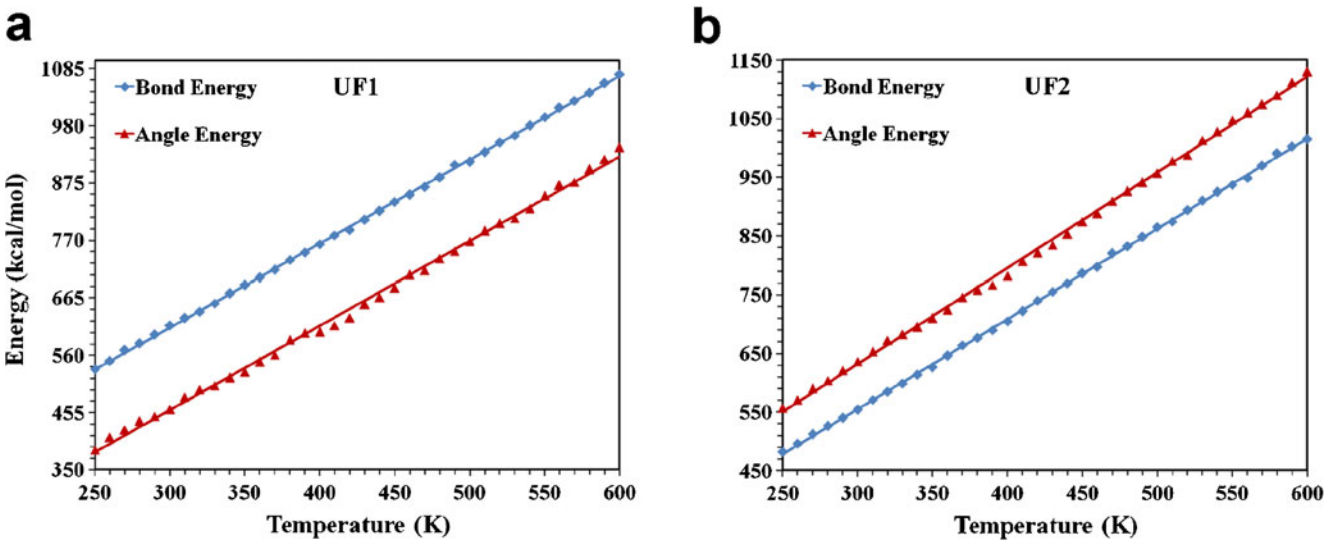

Fig. 6a–b Plots of the bond and angle energy components vs. temperature for **a** UF1 and **b** UF2

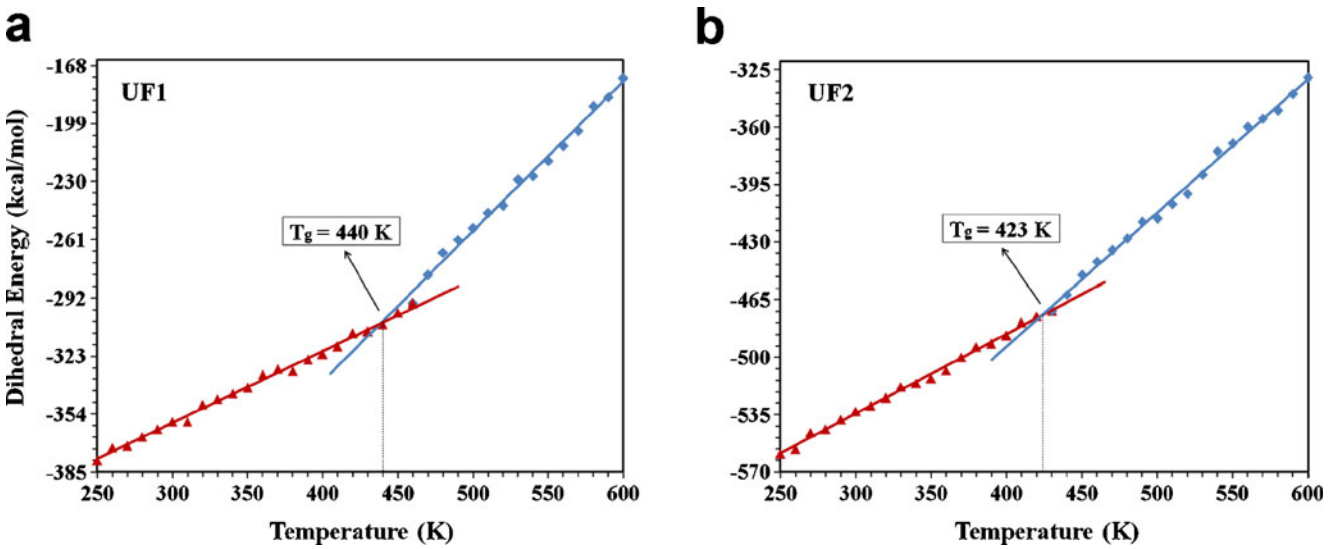

Fig. 7a–b Variation of the dihedral energy in terms of temperature for **a** UF1 and **b** UF2. The point of intersection between the fitted lines gives an estimate of the glass transition temperature (as shown on each plot)

glass transition region can be roughly estimated by searching for an unusually large gap between MSD–time curves that have been plotted over a range of temperatures, including T_g.

In the energy–temperature and property–temperature approaches, the changes in different energy components (bond, angle, dihedral, nonbonded, …) and also some polymer properties (density or specific volume, heat capacity, coefficient of thermal expansion, elastic modulus, …) with temperature are used to estimate the glass transition temperature.

Although the abovementioned approaches are independent and can be utilized individually, doing so results in rough and unreliable estimates of T_g. Hence, it is highly recommended that they should be used collectively in order to achieve more precise estimates of glass transition temperatures.

In order to apply all of these approaches in this study, the equilibrated structures were subjected to a temperature cycle as follows. They were heated from 300 K to 600 K through 1 ns (1000 ps) NPT dynamics. The systems were then gradually cooled to 250 K at a constant rate of 10 K/1000 ps through NPT dynamics and under atmosphere pressure, with each dynamics performed starting from the last structure and velocities obtained at the previous temperature. The temperature and pressure were controlled using the Nosé–Hoover method. In total, 36 trajectories, one per temperature, were generated and stored every 1 ps during the cooling-down dynamics. The generated trajectories were then used to establish and analyze the MSD–time, specific volume–temperature, and energy–temperature relationships and to calculate the glass transition temperature.

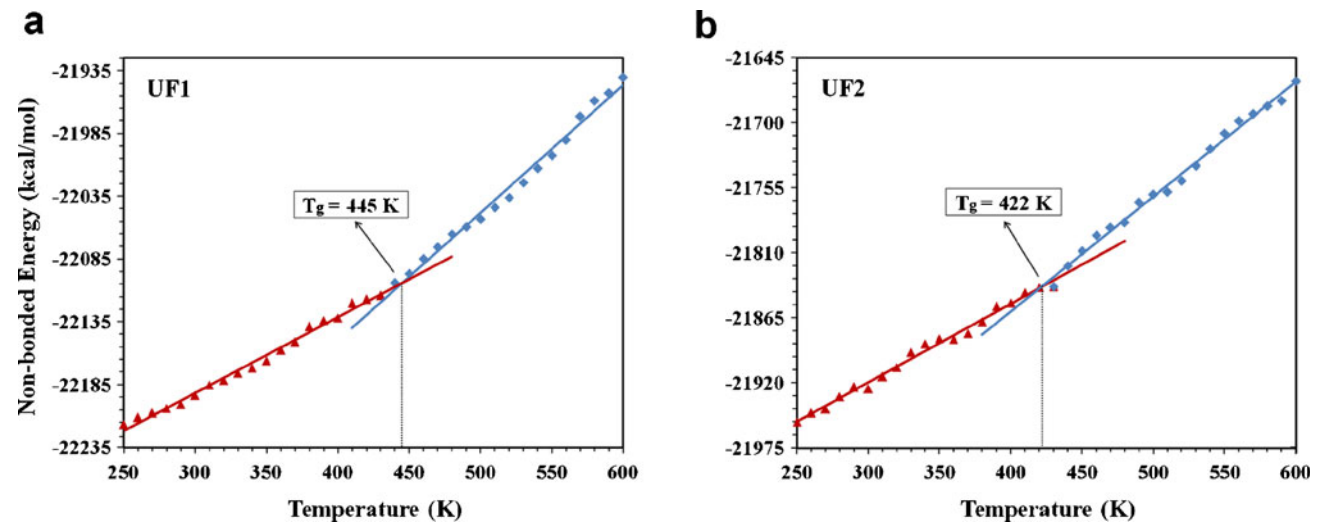

Fig. 8a–b Variation of the nonbonded energy with respect to temperature for **a** UF1 and **b** UF2. The point of intersection between the fitted lines gives an estimate of the glass transition temperature (as shown on each plot)

Results and discussion

Elastic constants

The elastic stiffness tensors of UF0, UF1, and UF2, obtained using the static method and averaged over the sampling trajectories, are provided below:

$$C_{ij}^{\mathrm{UF0}} = \begin{pmatrix} \mathbf{9.59} & \mathbf{4.64} & \mathbf{4.59} & 0.23 & 0.09 & 0.90 \\ \mathbf{4.64} & \mathbf{9.29} & \mathbf{4.55} & 0.15 & 0.03 & 0.67 \\ \mathbf{4.59} & \mathbf{4.55} & \mathbf{11.60} & 0.37 & 0.28 & 0.26 \\ 0.23 & 0.15 & 0.37 & \mathbf{2.81} & -0.14 & 0.05 \\ 0.09 & 0.03 & 0.28 & -0.14 & \mathbf{3.02} & -0.04 \\ 0.90 & 0.67 & 0.26 & 0.05 & -0.04 & \mathbf{2.69} \end{pmatrix} \mathrm{GPa}$$

$$C_{ij}^{\mathrm{UF1}} = \begin{pmatrix} \mathbf{15.35} & \mathbf{5.92} & \mathbf{6.36} & 0.06 & -0.04 & -0.74 \\ \mathbf{5.92} & \mathbf{14.84} & \mathbf{7.23} & -0.77 & 0.92 & -1.49 \\ \mathbf{6.36} & \mathbf{7.23} & \mathbf{17.77} & 0.18 & 0.45 & 0.10 \\ 0.06 & -0.77 & 0.18 & \mathbf{5.15} & -0.37 & 0.45 \\ -0.04 & 0.92 & 0.45 & -0.37 & \mathbf{4.76} & -0.52 \\ -0.74 & -1.49 & 0.10 & 0.45 & -0.52 & \mathbf{3.88} \end{pmatrix} \mathrm{GPa}$$

$$C_{ij}^{\mathrm{UF2}} = \begin{pmatrix} \mathbf{15.01} & \mathbf{7.12} & \mathbf{7.35} & 0.05 & 0.44 & 1.29 \\ \mathbf{7.12} & \mathbf{16.07} & \mathbf{6.42} & -0.25 & -0.23 & 0.65 \\ \mathbf{7.35} & \mathbf{6.42} & \mathbf{13.43} & -0.21 & 0.03 & -0.02 \\ 0.05 & -0.25 & -0.21 & \mathbf{4.27} & -0.07 & 0.02 \\ 0.44 & -0.23 & 0.03 & -0.07 & \mathbf{3.82} & -0.10 \\ 1.29 & 0.65 & -0.02 & 0.02 & -0.10 & \mathbf{4.76} \end{pmatrix} \mathrm{GPa}$$

We can confirm that the simulated systems are isotropic by considering the elastic tensors obtained. Although the components of the tensors that are not shown in boldface are not strictly zero, which is the case for isotropic materials, they are absolutely dominated by the components shown in bold, and the deviations of the estimated elastic constants from the values suggested by Eq. 3 are negligible. Furthermore, all of the stiffness tensors are symmetrical along the diagonal components. Therefore, the calculated elastic stiffness constants are reasonable and imply, to a good approximation, the behavior of an isotropic amorphous material. The moduli and Poisson's ratios of the simulated systems (as calculated using Eqs. 4a–d), along with the densities at 300 K, are reported in Table 1. The results are reasonable and in good agreement with experimental observations. The slight differences between the simulated and experimental values can be attributed to the quality and density of cross linking. In real conditions, the cross linking density (conversion rate) is usually less than 100 %, and the cross links are not always uniformly distributed within the material. In this study, however, the properties are calculated for perfect, highly cross-linked polymers, which is why the calculated properties are higher than those reported in the literature. The properties of cross-linked UF1 and UF2 show significant improvements over those of uncross-linked UF0. The differences between the properties of the UF1 and UF2 structures are mainly due to the different kinds of cross linkers used in these systems. In other words, the utilization of methylene cross linkers in UF1 led to better properties than the utilization of dimethylene ether cross linkers in UF2 did, which suggests that methylene should be the preferred cross linker in the synthesis of poly(urea-formaldehyde) capsules for self-healing materials.

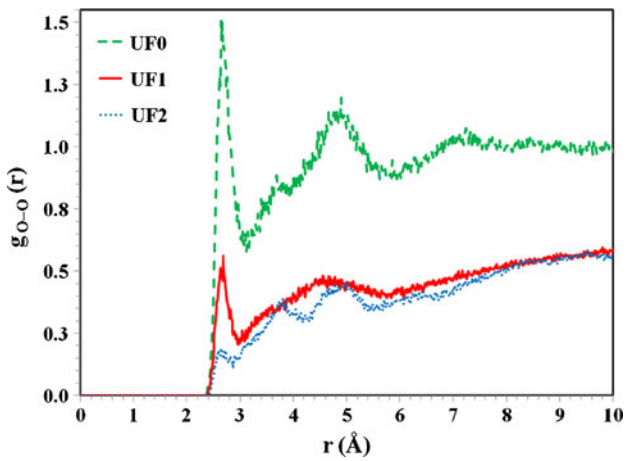

Fig. 9 Intermolecular O–O pair correlation functions for UF0, UF1, and UF2 at 300 K

Table 2 Glass transition temperatures—obtained using various approaches—of simulated cross-linked urea-formaldehyde polymers

Simulated structure	T_g (K)				
	MSD	Specific volume	Dihedral energy	Nonbonded energy	Average
UF1	440-460	443	440	445	442.67
UF2	420-440	430	423	422	425

Glass transition temperature

The initial 30 ps of the trajectories, which were generated during the cooling-down dynamics, were used to calculate

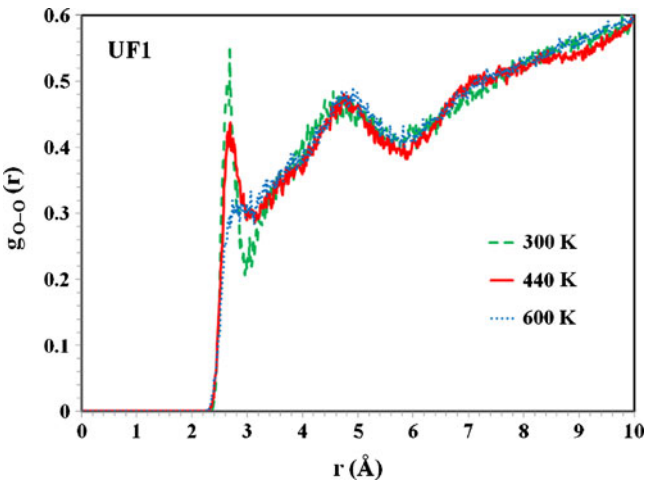

Fig. 10 Intermolecular RDFs of O–O pairs for UF1 at different temperatures: well below T_g (300 K), at around T_g (440 K), and well above T_g (600 K)

the MSD values in terms of time and temperature. The MSD–time curves of UF1 and UF2 are plotted every 20 K from 320 K to 520 K (the range of temperatures considered in this study) in Fig. 4. There are distinct gaps between the "upper" and the "lower" sets of MSD curves in the plots, which are due to increased kinetic energy of the atoms and chain disentanglement. The positions of the gaps in the plots yield rough estimates for the glass transition regions of UF1 and UF2: 440–460 K for UF1 (Fig. 4a) and 420–440 K for UF2 (Fig. 4b).

The specific volumes of the simulated systems were also obtained from the last 300 ps of NPT dynamics generated at each temperature during the cooling-down dynamics, and linear trend lines were fitted to the generated data points to study the specific volume-temperature relationship and accurately calculate the T_g. Figure 5 illustrates the variations in the specific volumes of UF1 and UF2 with respect to temperature. It is evident from Fig. 5 that the specific volume increases with increasing temperature, and the trend does not remain linear during the cooling-down stage. In other words, passing through the glass transition region results in changes in the slopes of the fitted trend lines. The point of intersection in each plot provides estimates of the glass transition temperatures for the simulated UF1 (T=443 K) and UF2 (T=430 K) systems. The values obtained are reasonably within the glass transition regions predicted by the MSD curves (Fig. 4).

The last 300 ps of the trajectories generated during the cooling-down NPT dynamics were again used to investigate the roles of different energy components in the glass transition behaviors of the simulated structures. The variations of different energy components as a function of temperature, including bond (stretching), angle (bending), dihedral (torsion), and nonbonded (van der Waals and electrostatic) energies, are discretely plotted in Figs. 6, 7, and 8. The variations in the bond and angle energies of UF1 (Fig. 6a) and UF2 (Fig. 6b) are almost linear and do not kink at any of the temperatures considered here. On the other hand, obvious bilinear trends are apparent in the plots of the dihedral (Fig. 7) and nonbonded (Fig. 8) energies. The changes in the slopes of the fitted trend lines are due to increased torsional and rotational degrees of freedom of the polymer chains during the transition from a glassy to a rubbery state. In other words, the flexibility of the polymer chains changes drastically as they pass through the glass transition region. The breakpoints on the dihedral energy plots yield T_g values of 440 K and 423 K for UF1 and UF2, respectively. From the nonbonded energy plots, the estimated glass transition temperatures for UF1 and UF2 are 445 K and 422 K, respectively. All of these values are reasonably within the temperature ranges suggested by the MSD curves. The estimated values of T_g obtained through the different approaches are summarized in Table 2. All of the approaches used in the current study predicted a higher glass transition temperature for UF1 than for UF2, which can be attributed to the types of cross linkers used in them. Similar to the elastic properties, as discussed in a previous subsection, the glass transition temperature is improved by the use of methylene cross linkers in UF1.

Hydrogen bonding

The radial distribution function (RDF) was used in order to investigate the influences of the cross linking and the temperature on the intensity of hydrogen bonding (H-bonding) in the structures of the simulated urea-formaldehyde polymers. The radial distribution function, also known as the pair correlation function, $g_{(r)}$, can be defined as the probability of finding a given particle at a distance r from a reference particle.

Although there is no explicit term for hydrogen bonding in the PCFF force field, the interaction is implicitly considered by tuning the LJ parameters for specific types of atoms [25]. Potentially available hydrogen donors and acceptors in UF0, UF1, and UF2 are oxygen in hydroxyl (−***O***H), nitrogen in primary and secondary amines (−***N***H_2 or −***N***H−), and oxygen in carbonyl (−C=***O***). The intermolecular RDFs between all pairs of polar atoms were analyzed; among them, the oxygen atoms were found to be the most significant contributors to the hydrogen bonding. The intermolecular correlations between oxygen atoms, calculated for distances of up to 10 Å, are plotted in Fig. 9. The first peaks at around 2.7 Å correspond to hydrogen bonds between polar O atoms in distinct chains, and the subsequent peaks correspond to other nonbonded interactions, including van der Waals and electrostatic interactions. It is evident from the figure that the intensity of H-bonds and other nonbonded interactions in uncross-linked UF0 is considerably greater than the corresponding intensity in the cross-linked UF1 and UF2 structures. This is clearly due to the creation of covalent bonds between the individual chains of pre-polymers and the reduction in the number of distinct molecules in the UF1 and UF2 networks. Moreover, the cross linking process leads to the loss of many oxygen and hydrogen atoms that contribute to the H-bonding. The magnitude of the first peak in the case of UF1 is more than that of UF2 because the hydroxyl groups lose their hydrogen atoms, and consequently their role in the H-bonding, in order to form dimethylene ether linkages in the UF2 structure.

Figure 10 shows the RDFs of oxygen atoms in UF1 at three different temperatures: well below T_g (300 K), at around T_g (440 K), and well above T_g (600 K). As expected, the magnitude of the first peak (attributed to the H-bonding) decreases with increasing temperature, and the peak shifts slightly towards longer distances. The same behavior was observed in the RDFs of the other pairs of polar atoms (i.e., N−N and O−N). These results are consistent with observations reported in [25, 26], and confirm that both the cross linking and the temperature influence the intensity of the hydrogen bonds in the cross-linked polymer structure.

Conclusions

In this study, molecular dynamics with the PCFF force field was utilized, for the first time, to simulate cross-linked poly(urea-formaldehyde) structures for use in self-healing materials. The constant strain (static) approach was then adopted to calculate the mechanical properties of the simulated structures. Comparing the simulation results with experimental data confirmed the accuracy of the models and the simulation procedure. Using the mean squared displacement (MSD) along with the specific volume–temperature and energy–temperature relationships, the glass transition behaviors of the simulated materials were investigated. The variations in the bond, angle, dihedral, and nonbonded energy components in terms of temperature were considered. Based on a rough estimation of the glass transition region, obtained from the MSD curve, more precise values of T_g were obtained from the bilinear trends in the specific volume and energy components versus temperature. In comparison to dimethylene ether linkages, methylene cross linkers were found to be more advantageous, as they led to significant improvements in the elastic constants and glass transition temperatures of the cross-linked urea-formaldehyde polymers.

Finally, the radial distribution function (RDF) was used to investigate the effects of cross linking and temperature on the hydrogen bonding present in the cross-linked PUF systems. The results revealed that increasing the temperature and cross linking density reduces the intensity of H-bonding in the studied polymers. Furthermore, hydrogen bonding was found to play a greater role in structures cross-linked through methylene linkages rather than dimethylene ether linkages.

Acknowledgments The authors would like to thank Prof. Antonio Pizzi (University of Lorraine, France) for helpful discussions. The High Performance Computing (HPC) Laboratory, Institute for Research in Fundamental Sciences (IPM), Tehran, Iran is also acknowledged for providing computational facilities for our simulations.

References

1. White SR, Sottos N, Geubelle P, Moore J, Kessler MR, Sriram S, Brown E, Viswanathan S (2001) Autonomic healing of polymer composites. Nature 409(6822):794–797
2. Blaiszik B, Sottos N, White S (2008) Nanocapsules for self-healing materials. Compos Sci Technol 68(3):978–986
3. Cho SH, White SR, Braun PV (2008) Self–healing polymer coatings. Adv Mater 21(6):645–649
4. Kirkby E, Michaud V, Månson JAE, Sottos N, White S (2009) Performance of self-healing epoxy with microencapsulated healing agent and shape memory alloy wires. Polymer 50(23):5533–5538
5. Rule JD, Sottos NR, White SR (2007) Effect of microcapsule size on the performance of self-healing polymers. Polymer 48(12):3520–3529
6. Suryanarayana C, Rao KC, Kumar D (2008) Preparation and characterization of microcapsules containing linseed oil and its use in self-healing coatings. Prog Org Coat 63(1):72–78
7. Yuan YC, Rong MZ, Zhang MQ, Yang GC (2009) Study of factors related to performance improvement of self-healing epoxy based on dual encapsulated healant. Polymer 50(24):5771–5781
8. Nesterova T, Dam-Johansen K, Kiil S (2011) Synthesis of durable microcapsules for self-healing anticorrosive coatings: a comparison of selected methods. Prog Org Coat 70(4):342–352
9. Yin T, Rong MZ, Zhang MQ, Yang GC (2007) Self-healing epoxy composites—preparation and effect of the healant consisting of microencapsulated epoxy and latent curing agent. Compos Sci Technol 67(2):201–212
10. Conner AH (2001) Wood: adhesives. In: Encyclopedia of materials: science and technology. Elsevier, New York
11. Pizzi A, Mittal KL (2003) Handbook of adhesive technology, revised and expanded edn. CRC, Boca Raton
12. Accelrys Inc. (2013) Materials Studio. Accelrys Inc., San Diego. http://accelrys.com/products/materials-studio
13. Plimpton S (1995) Fast parallel algorithms for short-range molecular dynamics. J Comput Phys 117(1):1–19
14. Sandia National Laboratories (2013) LAMMPS molecular dynamics simulator. Sandia National Laboratories, Albuquerque. http://lammps.sandia.gov
15. Sun H, Mumby SJ, Maple JR, Hagler AT (1994) An ab initio CFF93 all-atom force field for polycarbonates. J Am Chem Soc 116(7):2978–2987
16. Ewald PP (1921) Die Berechnung optischer und elektrostatischer Gitterpotentiale. Ann Phys 369(3):253–287
17. Shokuhfar A, Arab B (2013) The effect of cross linking density on the mechanical properties and structure of the epoxy polymers: molecular dynamics simulation. J Mol Model 19(9):3719–3731
18. Berendsen HJC, Postma JPM, Van Gunsteren WF, DiNola A, Haak J (1984) Molecular dynamics with coupling to an external bath. J Chem Phys 81:3684
19. Nosé S (1984) A molecular dynamics method for simulations in the canonical ensemble. Mol Phys 52(2):255–268
20. Hoover WG (1985) Canonical dynamics: equilibrium phase-space distributions. Phys Rev A 31(3):1695–1697
21. Theodorou DN, Suter UW (1986) Atomistic modeling of mechanical properties of polymeric glasses. Macromol 19(1):139–154
22. Choi J, Yu S, Yang S, Cho M (2011) The glass transition and thermoelastic behavior of epoxy-based nanocomposites: a molecular dynamics study. Polymer 52(22):5197–5203
23. Martienssen W, Warlimont H (2005) Springer handbook of condensed matter and materials data, vol 1. Springer, Berlin
24. Park B-D, Frihart CR, Yu Y, Singh AP (2013) Hardness evaluation of cured urea-formaldehyde resins with different formaldehyde/urea mole ratios using nanoindentation method. Eur Polym J 49:3089–3094. doi:10.1016/j.eurpolymj.2013.06.013
25. Yang S, Qu J (2012) Computing thermomechanical properties of crosslinked epoxy by molecular dynamic simulations. Polymer 53(21):4806–4817
26. Wu C, Xu W (2007) Atomistic molecular simulations of structure and dynamics of crosslinked epoxy resin. Polymer 48(19):5802–5812